AC operation and runaway electron behaviour in HT-7 tokamak*

Lu Hong-Wei(卢洪伟)†, Hu Li-Qun(胡立群), Zhou Rui-Jie(周瑞杰),
Lin Shi-Yao(林士耀), Zhong Guo-Qiang(钟国强), Wang Shao-Feng(王少锋),
Chen Kai-Yun(陈开云), Xu Ping(许 平), Zhang Ji-Zong(张继宗)
Ling Bi-Li(凌必利), Mao Song-Tao(毛松涛), Duan Yan-Min(段艳敏), and HT-7 Team

Institute of Plasma Physics, Chinese Academy of Sciences, Hefei 230030, *China*

(Received 4 September 2009; revised manuscript received 7 December 2009)

Operation of HT-7 tokamak in a multicycle alternating square wave plasma current regime is reported. A set of AC operation experiments, including LHW heating to enhance plasma ionization during the current transition and current sustainment, is described. The behaviour of runaway electrons is analysed by four HXR detectors tangentially viewing the plasma in the equatorial plane, within energy ranges 0.3–1.2 MeV and 0.3–7 MeV, separately. High energy runaway electrons (∼MeV) are found to circulate predominantly in the opposite direction to the plasma current, while the number of low energy runaway electrons (∼tens to hundreds of keV) circulating along the plasma current is comparable to that in the direction opposite to the plasma current. AC operation with lower hybrid current drive (LHCD) is observed to have an additional benefit of suppressing the runaway electrons if the drop of the loop voltage is large enough.

Keywords: runaway electron, alternating current (AC) discharge, lower hybrid current drive, loop voltage

PACC: 5225, 5255

1. Introduction

Alternating current (AC) operation of a tokamak reactor is an attractive regime to generate a continuous output of electric energy without the need for a complicated non-inductive current driven system. The use of AC inductive current drive for a tokamak fusion reactor allows the reactor to operate with a minimum plant recirculating power. Compared with non-inductive current drive operation, AC discharges are technically simpler and have higher cost efficiency.[1] A possible disadvantage of the AC regime could be mechanical fatigue of some tokamak components.[2] However, the achievement of long flat-top plasma current AC discharges can degrade the importance of this effect.[3] The potential problems associated with thermal fatigue of a first wall and a blanket and with mechanical fatigue of the toroidal coil may be relaxed by long-pulse operation with a half-cycle period of several hours using a large Ohmic transformer flux, perhaps > 1000 Vs. Thus AC operation will be a very important mode of operation for a next-step device such as the international thermonuclear experimental reactor (ITER) and commercial tokamak reactors as well.[4]

AC operation was first demonstrated in the STOR–IM tokamak,[5] at a plasma current level of 4 kA and a cycle time of 4 ms, and then fulfilled on several other devices with different current traces. Except for JET[6] (2 MA with a dwell time from 50 to 6 ms), all the other devices are operated with fairly low plasma current (several kA or so with zero or finite dwell time). These experiments are helpful for solving the problem of sustaining plasma current. Therefore, understanding these experiments is currently one of the key issues in tokamak fusion study, and it is also of interest for those who concern the final realization of controlled fusion energy.[7]

A quasi-steady-state multicycle alternating flat-top plasma current operation was achieved successfully with a duration of more than one minute on the HT-7 superconducting tokamak with plasma current $I_{\rm p} = 100$ kA, line-averaged density of $n_{\rm e} = 1.25 \times 10^{19}$ m^{-3} (0.1–0.4×10^{19} m^{-3} at the time of current transition), electron temperature $T_{\rm e} = 500$ eV, by the careful control of the configuration, intensified gas puffing, upgraded PF power supply system and the lower hybrid wave (LHW) assistance.[8] Plasma

*Project supported by the National Natural Science Foundation of China (Grant Nos. 10935004 and 10775041).

†Corresponding author. E-mail: luhw@ipp.ac.cn

© 2010 Chinese Physical Society and IOP Publishing Ltd

current, density and position were feedback controlled during the flat-top of plasma current.[1]

Although AC plasma has been performed on many tokamaks, the runaway electron behaviours in AC plasmas have not been widely discussed. In this paper, with the aid of the electron cyclotron emission (ECE), soft x-ray diagnostic system (SXR), vertical multi-channel hard x-ray diagnostic system (HXV) and the runaway electron diagnostic system (RA), the AC operation and the runaway electron behaviours in AC plasmas are presented, in detail, by comparing the two current directions (positive and negative). The effects of lower hybrid current drive (LHCD) and loop voltage on runaway electrons during AC plasma discharges are also discussed in detail separately.

The rest of the present paper is organized as follows. In Section 2, the experimental set-up is introduced. AC discharge with LHCD at the time of current transition is presented in Section 3. In Section 4, AC discharges with LHW during the current flat-top are presented and discussed in subsections: Subsection 4.1 is for AC discharges with LHW during the whole duration, Subsection 4.2 is for AC discharges with LHCD during the positive current phase and Subsection 4.3 is for AC discharges with LHW during the negative current phase. Finally the conclusions are drawn in Section 5.

2. Experimental set-up

Hefei Tokamak-7 (HT-7) which was rebuilt from the original Russian T-7 tokamak in 1994 is a medium-sized tokamak with superconducting toroidal coils and water-cooled graphite limiters, constructed to achieve high-performance long pulse plasma discharges and to study relevant physics. The machine runs normally with plasma current $I_{\rm p} = 100 - 225$ kA, toroidal magnetic field $B_{\rm T} = 1.5$–2 T, central line-averaged plasma density $n_{\rm e}$=(1–6)$\times 10^{19}$ m^{-3}, major radius $R = 122$ cm, minor radius $a = 27$ cm, central electron temperature $T_{\rm e}$=0.5–3.0 keV, and central ion temperature $T_{\rm i}$=0.2–1.5 keV, with a circular cross section.[9] The plasma current, position and central line-averaged electron density were feedback controlled during discharges. A stainless-steel liner was installed in the vacuum chamber at the radius of 0.32 m.[10,11]

The following basic diagnostics will be used in the paper.

A 35-channel H_α ($\lambda = 656.3$ nm) photodiode array is mounted on the top port to monitor the plasma, with the components including a lens, an interference filter, a 35-channel photo diode chip and the preamplifiers.[8] The soft x-ray diagnostic system consists of two imaging cameras with slot-apertures, through which a given toroidal cross-section of the plasma can be viewed from different poloidal chords horizontally and vertically, each camera containing 37 Au–Si surface-barrier diode detectors.[12,14] All detectors are mounted on the arc-shaped stainless-steel pedestals with $R = 55$ cm in a horizontal array and $R = 60$ cm in a vertical array. Thespatial resolution, the radial distance between neighbouring viewing chords of the detector, is 1.5 cm for each detector. They view the plasma from -27 cm to $+27$ cm along the given chords through thin slot-apertures with an area of 5×20 mm^2 in the vertical array and 4×25 mm^2 in the horizontal array. The time resolution ranges from about 4 μs to 12.8 μs.[15]

Vertical multi-channel hard x-ray (HXV) diagnostic system was composed of CdTe detectors. In an energy range of 20–300 keV, it has a moderate stopping efficiency and good energy resolution. And there is a 11-sight line set to observe the fast electron bremsstrahlung (FEB) emission in the poloidal cross section from +25 to –25 cm with a spatial resolution of 5 cm, and a sight line is set to monitor the wall radiation on the low field side. The shielding is provided by a 3-cm-thick homogeneous lead plate cast in one piece between two 4-mm-thick stainless steel plates. The pinhole has 4×4 mm square aperture, which can be changed into other dimensions manually. This system is installed in front of an aluminum vacuum window (1-mm thick), nearly transparent to photons with energy $E_\gamma > 20$ keV. A CdTe detector and a preamplifier are mounted in aluminum housing with dimensions of $20 \times 40 \times 50$ mm^{-3}, equipped with an aluminum entrance window (100-μm thick). The detection head is made of a spectroscopy grade CdTe detector ($5 \times 5 \times 2$ mm^{-3}).[16]

Recently, a broadband heterodyne radiometer has been installed on HT-7 tokamak to measure second harmonic x-mode electron cyclotron emission at a frequency range of 98–126 GHz, which is the only detectable ECE mode with an optical depth greater than 1 in the present study.[17] The high temporal resolution (4 μs) diagnostic system is now operational with 16 detection channels separated by approximately 2 cm on the radial axis for measuring electron temperature ($T_{\rm e}$) on the low-field side for a typical machine operation at a toroidal magnetic field ($B_{\rm T}$)

of 1.0–2.5 T.

The hard x-ray emission resulting from the thick target bremmstralung when runaway electrons are lost from the plasma and impinge on the vessel walls or plasma facing components[18] provides information about the generation, the loss and the energy content of runaway electrons.[19,20] And the system is mainly sensitive to the electrons leaving the plasma. Four hard x-ray detectors have been installed to monitor the runaway electrons with a tangential view into the plasma in the equatorial plane. The two NaI (TL) (ϕ50 mm×50 mm) scintillator detectors are used to monitor the high-energy hard x-ray radiation in an energy range of 0.3–7 MeV, and two CdTe detectors (hemispherical, with a volume of 65 mm^3 a diameter of 8 mm and a length of 91 mm) are used to monitor the low-energy hard x-ray in an energy range of 0.3–1.2 MeV. One of the NaI (TL) scintillator detectors (with the label RA3) and one of the two CdTe detectors (with the label RA1) are installed tangentially in the equatorial plane with the clockwise direction (for monitoring the hard x-ray emission of clockwise direction), while the other CdTe detector (with the label RA2) and the other NaI (TL) scintillator detector (with the label RA4) are installed tangentially in the opposite direction (anticlockwise direction) as shown in Fig. 1.

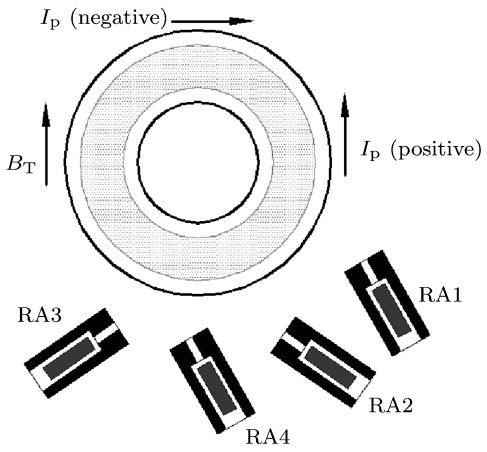


Fig. 1. Schematic of runaway electron diagnostics during AC plasmas on the HT-7 tokamak (down view).

The CdTe detectors (RA1 and RA2) are installed inside a lead shielding against uncollimated x-ray radiation. An entrance hole (with a radius of 1 cm and a length of 2 cm) is made in the front of the lead shielding to collimate hard x-ray radiation. The entrance hole of the lead shielding of RA1 has the same size as that of RA2. The cylindrical lead shieldings of NaI (TL) scintillator detectors (RA3 and RA4) are both 11 cm in radius, 40 cm in length and 10 cm in thickness. An entrance hole of the collimator is about 1 cm in radius and 15 cm in depth. Photomultipliers are usually influenced by magnetic field. Two soft iron cylinders closely housing the photomultiplier tube are used to shield stray field from the tokamak coils. A data acquisition system provides the integrated hard x-ray emission flux by detecting the photomultiplier anode current.[21]

The current directions are defined in the bird's eye view[22] as shown in Fig. 1. The positive current is in the anticlockwise direction and the negative current is in the clockwise direction. The toroidal field direction is kept in the clockwise direction during all of the AC discharges as shown in Fig. 1.

3. AC discharge with LHCD at the time of current transition

Figure 2 shows a typical steady-state AC discharge (shot No. 99552) with lower hybrid current drive (LHCD) only at the time of current transition on the HT-7 tokamak. The plasma current is fixed at about 100 kA for both the positive and negative current directions. The central line-averaged density is about 1.25×10^{19} m^{-3}, and it slightly changes during the flat-top plasma current. The line-averaged density of the positive current plasma is almost the same as that of the negative current plasma. Central electron temperature T_e is 500 eV. To keep the gas ionized at the phase of current transition, the gas puffing pulse and the power of 250-kW LHCD are applied in a way as shown in Fig. 2. During current flat top, feedback gas puffing is employed to keep plasma density at a required value. We can see from Fig. 2 that H_α line emission intensity in the positive phase is twice as high as that in the negative phase (from 0.4 to 0.2 in arbitrary units). These observations, taking into consideration the slight difference in line average density between both current phases (Fig. 2), suggest that the particle confinement of the positive plasma is lower than that of the negative current plasma.[22]

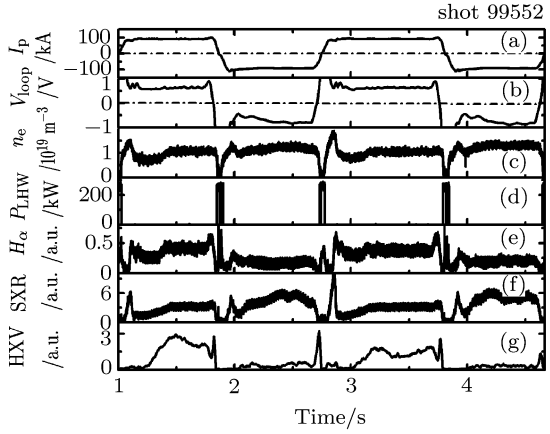


Fig. 2. Typical AC discharge (shot No. 99552) with lower hybrid current drive (LHCD) only at the time of current transition, showing the traces: (a) plasma current, (b) loop voltage, (c) central line-averaged density, (d) LHCD power, (e) H_α line emission, (f) soft x-ray emission detected by photodiode array, (g) FEB detected by the CdTe array inside the vessel (vertical position.)

The difference in behaviour of the runaway electrons in between the positive and the negative current directions is interesting and has rich connotations of physics. Figure 3 shows the traces of emission signal in shot No. 99552. We can see from the figure that RA1 and RA2 signals increase at 1.2 s while the RA3 and RA4 are negligible. The increase of the emission in the low energy RA1 and RA2 detectors is correlated to the generation of runaway electrons during the current ramp-up, while the high energy RA3 and RA4 signals are still close to zero, which is possibly because the runaway electron energy is too low to give noticeable emission. The later increases of the signals in all the detectors at about 1.2–1.3 s are due to the acceleration and energy gain (possibly including avalanche runaway generation) of the runaway electrons during the flat-top phase. The runaway electrons are generated during the ramp-up of the current by the Dreicer process, when the loop voltage is larger and the density is lower. During the flat-top phase, the number of Dreicer process generated runaway electrons seems to be negligible. Parameter $\varepsilon = E_\parallel/E_c = E_\parallel(4\pi\varepsilon_0^2 kT_e/ne^3\ln\Lambda)$ can determine the Dreicer process generated runaway electron yield during the flat-top and it is estimated by using $E_\parallel \sim V_l/2\pi R_0$ with $V_l \sim 0.7$ V and $R_0 = 122$ cm $n_e = 1.25\times10^{19}$ m^{-3} and $\ln\Lambda \cong 15$, i.e. $\varepsilon = 0.011$, which is too low to allow for runaway generation (the primary generation generally works for $\varepsilon > 0.02$[23]). As long as $\varepsilon < 002$, only an exponentially small fraction of the electrons will run away. The traces of the calculated critical energy for runaway generation, $W_c(t)$ ($W_c = (e^3 n_e \ln\Lambda(2+Z_{eff}))/8\pi\varepsilon_0^2 E$, using $E_\parallel \sim V_l/2\pi R$), the parameter $\varepsilon(t)$, the secondary runaway electron birth rate ($(\mathrm{d}n_{r,sec})/(\mathrm{d}t) = (3n_r eEc)/(2m_0c^2\ln\Lambda(2+Z_{eff}))$, which is independent of electrons density n_e) and the avalanche time for secondary runaway generation[24] ($\tau_s = (2(2+Z_{eff})m_e c\ln\Lambda)/3eE$), where $n_{r,sec}$ is the number of secondary runaway electrons, E is the inductive electric field, Z_{eff} is the effective ion charge, n_r is the total number of runaway electrons for shot No. 99552 according to the experimental data are shown in Fig. 4 (using $T_e = 500$ eV, $\ln\Lambda = 15$, $R_0 = 122$ cm and $Z_{eff} = 2$). From the figure we can see that the critical energy for runaway generation W_c is about 110 keV and parameter ε is about 0.01 during the flat-top phase, both the positive phase and the negative phase, while it was not the case during the current transition (W_c becomes very low and $\varepsilon > 0.02$). Therefore, we can see that the runaway electron generating Dreicer process plays a more important part in the current ramp-up phase, while the avalanche (secondary) process (the creation of runaways through close collisions of already existing runaways with thermal electrons) plays an important role in the current flat-top phase. We can also see from Fig. 4 that the avalanche process plays a more important role than Dreicer process during the current transition because of the high inductive loop voltage. And it ($\mathrm{d}n_{r,sec}/\mathrm{d}t$) decays during

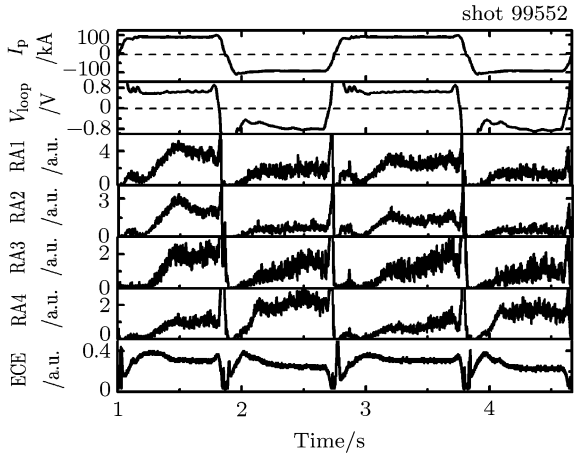


Fig. 3. Traces of emission signal in shot No. 99552 (from top to bottom): plasma current loop voltage in detail, HXR intensity measured by a CdTe detector in the clockwise direction (RA1), HXR intensity measured by a CdTe detector in the anticlockwise direction (RA2), HXR intensity measured by a NaI (TL) scintillator detector in the clockwise direction (RA3), HXR intensity measured by a NaI (TL) scintillator detector in the anticlockwise direction (RA4) and the signal of electron cyclotron emission (ECE).

the ramp-up phase. The avalanche time in the flat-top phase (see Fig. 4) $\tau_{\rm s} \approx 0.75$ s is a bit lower than that in the current ramp-up phase where $E_{\|} \sim V_l/2\pi R_0$ with $V_l \sim 0.7$ V, $\ln \Lambda = 15$, $Z_{\rm eff} = 2$ have been used. However, there are several effects that complicate the issue. Firstly, shortly after breakdown the plasma is only partially ionized whereas the theory treats only fully ionized plasmas. Secondly, in that phase of the discharge the distribution function of the bulk electrons may deviate strongly from a Maxwellian distribution. Thirdly, because of the relatively slow penetration of the applied electric field, it is most likely that in the startup phase the runaway electrons are generated predominantly in the outer region of the plasma.[25]

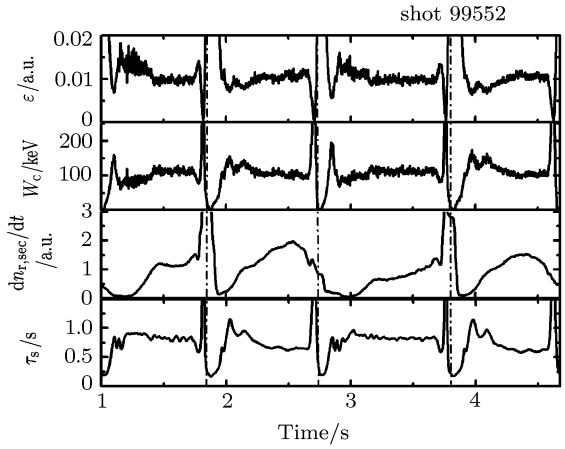


Fig. 4. Traces from top to bottom: calculated critical energy for runaway generation $W_{\rm c}(t)$, parameter $\varepsilon(t)$ determining the yield of runaway electrons generated by Dreicer process, the secondary runaway electrons birth rate ($\mathrm{d}n_{\rm r,sec}/\mathrm{d}t \sim n_{\rm r}E \sim RA \cdot V_{\rm loop}$, where RA signal shows the time evaluation of runaway electrons during the discharge under the assumption of a constant loss rate, $V_{\rm loop}$ signal indicates the time evaluation of induced electric field), and the avalanche time for secondary runaway generation ($\tau_{\rm s} = (2(2 + Z_{\rm eff})m_{\rm e}c \ln \Lambda)/3eE$) in shot No. 99552 according to the experimental data.

The HXR signals shown in Fig. 3 saturate at about 1.5 s. The reason is that the runaway electrons have already achieved their energy limit and/or the maximum energy that can be detected by the system (~ 7 MeV). To keep a runaway electron confined within the plasma, a sum of their orbit shift and drift orbit radius must be smaller than the minor radius a.[26] This limits the maximum runaway energy to $W_{\rm max} = aec\,B_0 = q_a$, where q_a is the edge safety factor. The orbit shift limit for HT-7 is $W_{\rm max} \sim 40$ MeV ($q_a = 4$, $B_0 = 2$ T). On the other hand, the estimated runaway energy limit in the core plasma is ~ 26 MeV while the edge runaway energy is blocked to a few MeV due to the strong interaction with the magnetic field ripple.[26]

We can also see from Fig. 3 that the loop voltage (both in the positive and the negative phases) is about 0.7 V: a little more than 0.7 V at the beginning of the negative current phase, and a little less than 0.7 V at the end of the negative current phase. The emission of high energy runaway electrons (RA3) in a clockwise direction is slightly larger in the positive current phase, while the emission of high energy runaway electrons (RA4) in an anticlockwise direction is larger in the negative current phase. These observations suggest that high energy (∼MeV) runaway electrons are mostly circulating in the opposite direction to the plasma current. This is consistent with the fact that high energy runaway electrons are basically collisionless and hence, essentially accelerated by the electric field in the opposite direction to the current direction. However, the intensities of low energy hard x-ray emission both in RA1 and RA2 detectors shows a similar time behaviour and the emission is larger in the positive current phase, suggesting that a more comparable number of low energy (∼tens to hundreds keV) runaway electrons are flowing in the direction opposite to the plasma current. It should be taken into account that lower energy runaway electrons are more collisional and have a larger probability of backscattering through their collisions with thermal electrons.

4. AC discharges with LHW during the current flat-top

In addition to maintaining steady state currents, the lower hybrid waves have also been used to start up and ramp up the tokamak plasma current as well as to heat electrons during LHCD experiments.[27] It is found that in the HT-7 tokamak, the electron runaway is enhanced in the presence of lower hybrid waves when the fast electron tail of velocity distribution extends to above the critical velocity for electrons to run away. In runaway discharges, the LHWs may suppress runaway electrons due to the drop in the electric field linked to the non-inductive current drive.[28]

In AC plasmas, besides helping plasma ionization during the current transition and current sustainment, AC operation with LHCD could have an additional benefit of suppressing the runaway electrons if the drop of the loop voltage is large enough. An LH power ($P_{\rm LH}$) up to 1.2 MW at 2.45 GHz is available presently

in the HT-7 machine. The launched parallel refractive index, $N_{\parallel}^{\rm peak}$, of LHWs can be varied from 1.8 to 3.5 with an FWHM of about 0.5, which provides flexibility for current density profile control.[29] The corresponding energy of the suprathermal resonant electrons is about 20–110 keV.

In the reported experiments, LHW heating is applied in the whole discharge duration (Subsection 4.1) as well as in one current phase (Subsections 4.2 and 4.3). In all the cases, the LHWs are injected to drive current in the positive current direction.

4.1. AC discharge with LHCD in the whole duration

A typical AC discharge with LHCD in the whole duration of the discharge (shot No. 99660) is shown in Fig. 5. The 200-kW LHW power was launched into the plasma from 0.1 s continuously, obtaining plasma current $I_{\rm p} = 100$ kA and central line-averaged density $n_{\rm e} = 1.25 \times 10^{19}$ m^{-3}. It should be noted that the low loop voltage (~ 0.25 V) in the positive current phase, associated with the creation of non-inductive current during LHCD, is much lower than the loop voltage in the negative current phase (~ 0.75 V). As a consequence, the generation of runaway electrons in the positive current phase (via the Dreicer mechanism and the avalanche process) will be quite smaller.

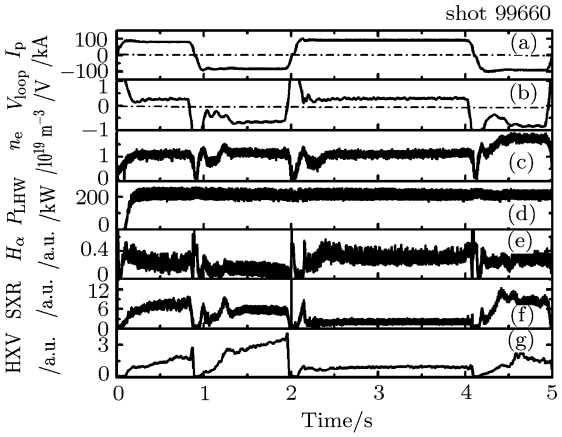


Fig. 5. Typical AC discharge (shot No. 99660) with lower hybrid wave (LHW) in the whole duration of the discharge, showing the traces: (a) plasma current, (b) loop voltage, (c) centre line-averaged density, (d) LHW power, (e) H_α line emission, (f) soft x-ray emission detected by photodiode array, (g) FEB detected by the CdTe array inside the vessel (vertical position.)

From Fig. 6 we can see that the critical energy for runaway generation $W_{\rm c}$ is about 30 keV in the positive phase, while $W_{\rm c} \cong 110$ keV in the negative phase. Concerning parameter ε that determines the yield of runaway electrons generated by the Dreicer process, its value equals 0.003 in the positive phase which is much lower than that ($\varepsilon = 0.01$) in the negative phase. The avalanche time is large in the positive current phase, when the loop voltage (and, hence, the electric field) is low, so that no secondary generation occurs in such a phase. The runaway avalanche generation yield in the positive phase is lower than that in the negative phase because the loop voltage in the positive phase is lower than that in the negative phase. And the avalanche production rate is very high only at 1.3–2 s.

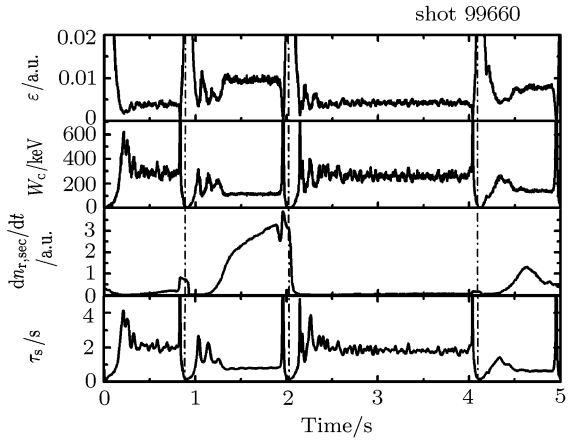


Fig. 6. Traces from top to bottom: parameter determining the yield of runaway electrons generated by Dreicer process, calculated critical energy for runaway generation $W_{\rm c}(t)$, secondary runaway electron birth rate ($dn_{\rm r,sec}/dt \sim n_{\rm r}E \sim RA \cdot V_{\rm loop}$, where RA signal shows the time evaluation of runaway electrons during the discharge under the assumption of a constant loss rate, $V_{\rm loop}$ signal indicates the time evaluation of inductive electric field) and the avalanche time for secondary runaway generation ($\tau_{\rm s} = (2(2 + Z_{\rm eff})m_{\rm e}c \ln \Lambda)/3eE$) in shot No. 99660 according to the experimental data.

The hard x-ray signals (RA1–RA4 detectors) are shown in Fig. 7. It is observed that in the positive current phase (with LHCD), the signals from the high energy detectors, RA3 and RA4, fall to zero while the low energy signals from RA1 and RA2 decay to a low level. This is mainly a consequence of the fall of the loop voltage and, hence, of the runaway electron energy in this phase. We can see from Fig. 7 that the loop voltage is about 0.25 V in the positive current phase, and it is about 0.75 V in the negative current phase. The average plasma density in the positive current phase is almost the same as that in the negative current phase. The low energy hard x-ray emission intensity in the positive current phase (both RA1 and RA2) is lower than that in the negative current phase

because of the low loop voltage in the positive current phase.

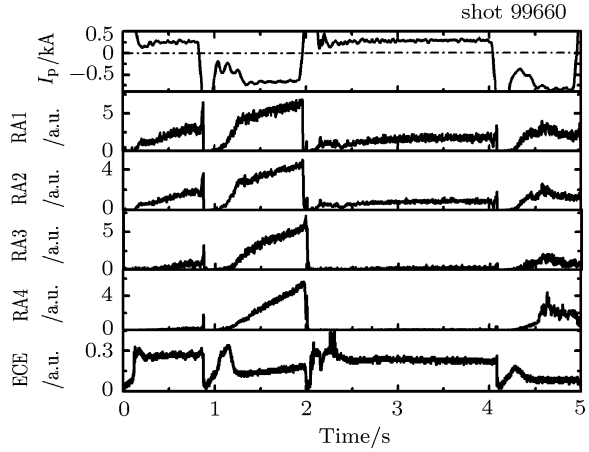


Fig. 7. Traces of emission signal in shot No. 99660 (from top to bottom): loop voltage in detail, HXR intensity measured by a CdTe detector in the clockwise direction (RA1), HXR intensity measured by a CdTe detector in the anticlockwise direction (RA2), HXR intensity measured by an NaI (TL) scintillator detector in the clockwise direction (RA3), HXR intensity measured by an NaI (TL) scintillator detector in the anticlockwise direction (RA4), and the signal of electron cyclotron emission (ECE).

In the negative current phase, due to the higher electric field, the yield of runaway electrons and the energy of the generated runaway electrons both increase, and the resulting emission intensities measured by the hard x-ray detectors (RA1–RA4) are substantially large. As the observations reported in Section 3 show, even though the runaway electrons in this phase are accelerated by the electric field in the counterclockwise direction (opposite to the plasma current), large emission intensities are also measured not only by RA2 and RA4 but also by RA1 and RA3 detectors, which is possibly due to the collisions of low energy (∼tens to hundreds of keV) runaway electrons with the thermal electrons which could reverse their flow direction.

Finally, the ECE emission (see Fig. 7) is observed to decrease in the negative current phase of the discharge. In a low density discharge, the plasma is optically thin and the ECE signal is mainly determined by the cyclotron radiation of the suprathermal electrons. When the electrons are accelerated by the electric field in the negative current phase, because of the high energy, the effect of the collisions is small, the pitch angle is low, and the radiation associated with the cyclotron motion can be reduced thereby reducing the ECE emission intensity. In contrast, in the positive current phase, due to the lower electric field and electron energy, pitch angle scattering due to the collisions with thermal plasma increases, leading to a larger ECE emission intensity

4.2. AC discharge with LHCD at the time of positive current

Figure 8 shows a typical AC discharge (shot No. 102994) with LHCD only in the positive current direction. The plasma current is about 100 kA for both the positive and the negative current phases. The trace of HCN is the original signal of the far infrared laser interferometer system which is used to measure the plasma density. The fixed central line-averaged density of this shot is about 1.25×10^{19} m^{-3} slightly changes during the time of 6 s–8 s (about 1.40×10^{19} m^{-3}). The plasma density is kept at about 0.1–0.4×10^{19} m^{-3} when the plasma current is zero.[1] The 250-kW LHW power is launched into the plasma in the positive current phase which is used to ionize plasma in the transition phase and drive the plasma current in the current flat-top phase.

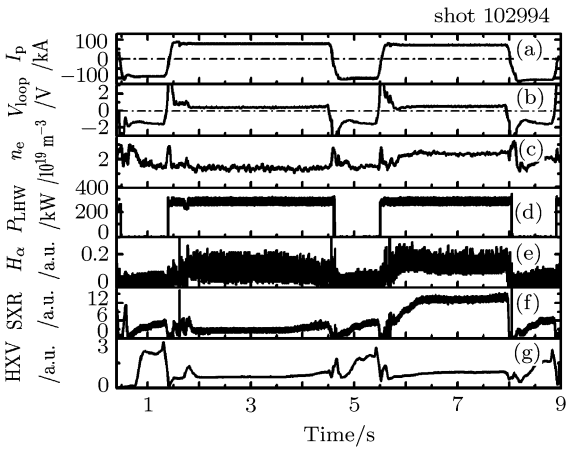


Fig. 8. Typical AC discharge (shot No. 102994) with lower hybrid current drive (LHCD) only in the positive current phase, showing the traces: (a) plasma current, (b) loop voltage, (c) original signal of the far infrared laser interferometer system, (d) LHCD power, (e) H_α line emission, (f) soft x-ray emission detected by photodiode array, and (g) FEB detected by the CdTe array inside of the vessel (vertical position.)

The LHCD takes place in the positive current phase and a fall of the electric field is found ($V_l \sim$ 0.4 V) which substantially reduces the runaway production ($W_c \sim 210$ keV in the positive current phase, while $W_c \sim 57$ keV in the negative current phase) and the runaway energy, leading to the disappearance of the MeV runaway population in this phase. Accordingly, the RA1–RA4 signals drop to zero (only low

RA1 and RA2 signals are observed in Fig. 9 in the second positive phase). In the negative current phase (no LHW injection), the intensities of hard x-ray emission in the four detectors (RA1–RA4) are very strong (see Fig. 9) because of the high loop voltage in this phase. Finally, the ECE signal noticeably drops in the negative current phase. Due to the large electric field, the electrons are accelerated to high energies in this phase, so that collisional pitch angle scattering and the radiation associated with the electron gyromotion are remarkably reduced.

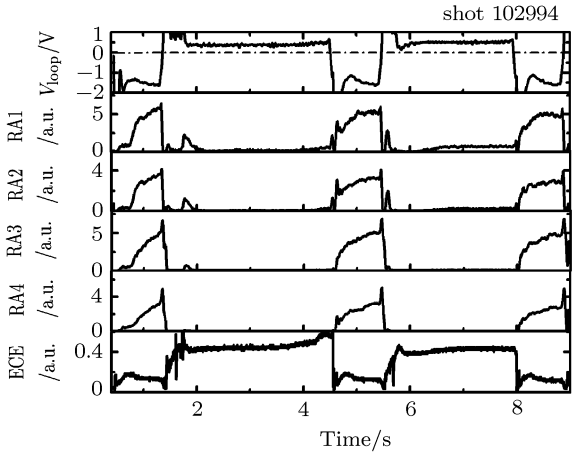


Fig. 9. Traces of emission signal in shot No. 102994 (from top to bottom): loop voltage in detail, HXR intensity measured by a CdTe detector in the clockwise direction (RA1), HXR intensity measured by a CdTe detector in the anticlockwise direction (RA2), HXR intensity measured by an NaI (TL) scintillator detector in the clockwise direction (RA3), HXR intensity measured by an NaI (TL) scintillator detector in the anticlockwise direction (RA4) and the signal of electron cyclotron emission (ECE).

It should be noted that in the negative current phase (no LHW), the loop voltage (~ 1.5 V) is much larger than that in shot No. 99552 (~ 0.7 V; see Fig. 2) also without LHW injection. The reason is that as indicated by soft x-ray and ECE emission measurements, the electron temperature in the negative current phase of short No. 102994 is smaller than that of shot No. 99552 and, hence, the plasma resistivity ($\eta \propto T^{-3/2}$) and the electric field both increase.

We can see from Fig. 9 that the loop voltage in the positive current phase (about 0.3 V) is lower than that in the negative current phase (about 1.5 V) because of the effect of LHCD on the plasma. So in the positive current phase, the hard x-ray emission intensities measured by the four detectors (RA1, RA2, RA3, and RA4) are all small because of the low loop voltage, while in the negative current phase, the hard x-ray emission intensities from the four detectors are all very strong because of the high loop voltage. From ECE signal we can find that the intensity of ECE in the positive current phase is stronger than that in the negative current phase. That is to say, in the positive current phase most of the super thermal electrons cannot be accelerated into runaway electrons by the low loop voltage because of the big drag forces (collisions damp) and big runaway critical energy, while in the negative current phase most of the super thermal electrons were accelerated into runaway electrons because of the high loop voltage and small runaway critical energy

4.3. AC discharge with LHW at the time of negative current

The trace of a typical AC discharge with LHW only in the negative current phase (shot No. 103006) is shown in Fig. 10. From the figure we can see that the plasma currents in the positive current phase and in the negative current phase are both about 100 kA. The fixed central line-averaged density of this discharge is also about 1.25×10^{19} m^{-3} (the same as that of shot No. 102994) and slightly changes in the discharge duration. The 250-kW LHW power is launched into the plasma in the negative current phase to ionize and heat the plasma. The critical energy for runaway generation in the positive phase is calculated to be $W_c \cong 80$ keV by using $V_l \sim 1.1$ V, while $W_c \cong 123$ keV in the negative phase by using $V_l \sim 0.7$ V.

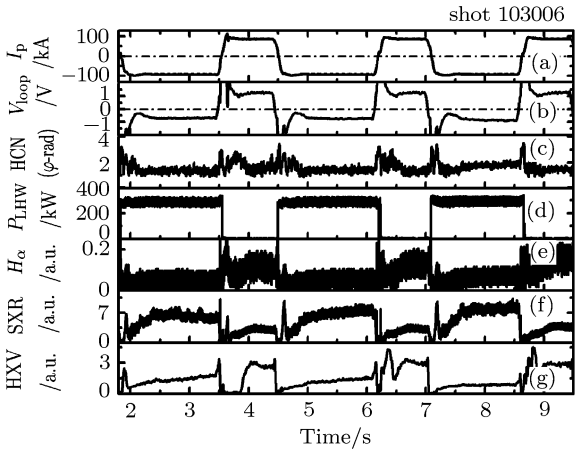


Fig. 10. Typical AC discharge (shot No. 103006) with lower hybrid wave (LHW) only in the negative current phase, showing the traces: (a) plasma current, (b) loop voltage, (c) original signal of the far infrared laser interferometer system, (d) LHW power, (e) H_α line emission, (f) soft x-ray emission detected by photodiode array, and (g) FEB detected by the CdTe array inside of the vessel (vertical position).

In the positive current phase (no LHW) in shot No. 103006, the voltage (~ 1.1 V) is also much larger than that (0.7 V) in shot No. 99552 shown in Fig. 2 also without LHW injection. The reason is also that the Spitzer resistivity

$$\eta_{\rm s} = 0.51 \frac{m_{\rm e}^{1/2} e^2 \ln \Lambda}{3\varepsilon_0^2 (2\pi T_{\rm e})^{3/2}} \sim T_{\rm e}^{-3/2}$$

decreases rapidly with the increase of electron temperature $T_{\rm e}$. We can see from Figs. 2 and 10 that the plasma currents and the line-averaged densities of these two shots are almost the same, while the SXR emission (0.2–0.3 in arbitrary units) in the positive current phase of shot No. 103006 was lower than that in the positive current phase of shot No. 99552 which is about 0.3–0.4 in arbitrary units. And the intensity of ECE signal (0.2 in arbitrary units) in the positive current phase of shot No. 103006 is weaker than that (0.4 in arbitrary units) in shot No. 99552. Therefore temperature $T_{\rm e}$ of shot No. 103006 in the positive current phase is lower than that in the positive current phase of shot No. 99552. And the Spitzer resistivity $\eta_{\rm s}$ in the positive current phase of shot No. 103006 is higher than that of shot No. 99552 in the positive current phase. Therefore the loop voltage ($V_l = 2\pi R_0 \eta . j$) in the positive current phase of shot No. 103006 (no LHW) is larger than that of shot No. 99552 shown in Fig. 2 also without LHW injection, because of the higher Ohmic power in shot No. 103006 in order to maintain the same current as that of shot No. 99552.

Comparing Fig. 11 with Fig. 9, we can find that the loop voltage in the positive current phase in Fig. 11 (which is about 1.4 V) and that in the negative current phase in Fig. 9 (which is about 1.5 V) are comparable. While the loop voltage in the negative current phase in Fig. 11 (which is about 0.8 V) is much higher than that in the positive current phase in Fig. 9 (which is about 0.3 V), even though the plasmas both in the negative current phase in Fig. 11 and in the positive current phase in Fig. 9 are heated by the same power of LHW and with maintaining the same central line-averaged density, with the slight change of the density in the flat-top phase neglected. We can also see in Fig. 7 that the loop voltage in the negative current phase (which is about 0.75 V) is higher than that in the positive current phase (which is about 0.25 V), even though the plasmas both in the negative current phase and in the positive current phase are heated by the same power LHW (200 kA) and with maintaining the same central line-averaged density ($n_{\rm e} = 1.25 \times 10^{19}$ m^{-3}). The possible reason may be that for LHW, the waves are launched with an asymmetric spectrum in $k_{\|}$ ($n_{\|}$) in a given toroidal direction, therefore the waves push forward the resonant electrons and thus drives a current only in one direction. The low hybrid waves are injected to drive a current only in the positive direction. LHCD will occur only in the positive phase of the current, while LHW heating takes place only in the negative phase of the current.

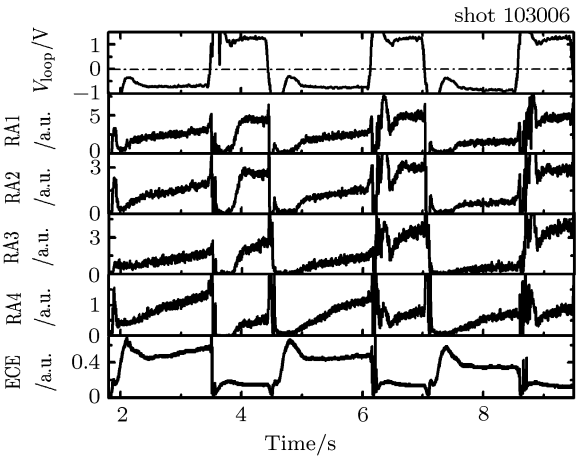


Fig. 11. Traces of emission signal in shot No. 103006 (from top to bottom): loop voltage in detail, HXR intensity measured by a CdTe detector in the clockwise direction (RA1), HXR intensity measured by a CdTe detector in the anticlockwise direction (RA2), HXR intensity measured by an NaI (TL) scintillator detector in the clockwise direction (RA3), HXR intensity measured by an NaI (TL) scintillator detector in the anticlockwise direction (RA4), and signal of electron cyclotron emission (ECE).

5. Conclusions

A quasi-steady state AC plasma operation is achieved successfully at about $I_{\rm p} = 100$ kA, $n_{\rm e} = 1.25 \times 10^{19}$ m^3, and $T_{\rm e} = 500$ eV in the HT-7 superconducting tokamak. The LHW heating is applied in the whole discharge duration and only in one current phase to enhance the plasma ionization during the current transition and current sustainment.

The behaviour of the runaway electrons during AC operation is analysed by four hard x-ray detectors tangentially viewing the plasma in the equatorial plane, within energy ranges of 0.3–1.2 MeV and 0.3–7 MeV, separately. Runaway electrons generating Dreicer process plays an important role during the current ramp-up of each current phase, while the

avalanche generation process seems to play a role during the current flat-top. High energy runaway electrons ($\sim$ MeV) are found to circulate mostly in the opposite direction to the plasma current, while the number of low energy runaway electrons (about tens to hundreds of keV) circulating along the plasma current is comparable to that in the direction opposite to the plasma current. AC operation with the lower hybrid current drive shows that besides helping plasma ionization during the current transition and current sustainment, the lower hybrid current drive can suppress the high energy runaway electrons in the current drive phases if the drop of the loop voltage is large enough.

References

[1] Li J G, Luo J R, Wang S J, Fu P, Shen B, Liu F K, Wan B N, Shan J F, Xu G S, Huang J, Yu J, Hu J S, Yuan Q P, Hu Y M and HT-7 Team 2007 *Nucl. Fusion* **47** 1071

[2] Cabral J A C, Fernandes H, Figueiredo H and Varandas C A F 1997 *Nucl. Fusion* **37** 1575

[3] Mitarai O, Wolfe S W, Hirose A and Skarsgard H M 1989 *Fusion Technol.* **15** 204

[4] Mitarai O, Conway G, Hirose A, Skarsgard H M, Xiao C, Zhang L and Zhang W 1993 *Plasma Phys. Control. Fusion* **35** 711

[5] Mitarai O, Wolfe S W, Hirose A and Skarsgard H M 1987 *Nucl. Fusion* **27** 604

[6] Tubbing B J D, Gottardi N A C, Green B J, How J A, Huart M, Konig R, Lowry C G, Lomas P J, Noll P, Orourke J J, Pebut P H, Stork D, Tanga A, Taroni A and Ward D J 1992 *Nucl. Fusion* **32** 967

[7] Wang S J 2004 *Phys. Rev. Lett.* **93** 155007

[8] Gao W, Gao X, Wu Z W, Yang J H and Zhang L 2008 *Plasma Phys. Control Fusion* **50** 115003

[9] Wan B N, Shi Y J, Xu G S, Gong X Z, Qian J P, Zhao Y P, Shan J F, Zhao J Y, Hu L Q, Li J G, Kuang G L, Lü B, Ling B L, Wu Z W, Liu F K, Mao Y Z, Gao X, Jie Y X, Mao J S, Zhou Q, Huang J, Xie J K and HT-7 Team 2003 *Phys. Plasma* **11** 2543

[10] Gao X, Xu Q, Li J G, Shan J F, Hu L Q, Zhao J Y and HT-7 Team 2008 *Plasma Phys. Control Fusion* **50** 035006

[11] Kuang G L, Liu Y X, Shan J F, Xu W H, Zhang X Q, Liu D C, Liu F K and Zhu Y B 1999 *Nucl. Fusion* **39** 1769

[12] Ma T P, Hu L Q and Chen Z Y 2005 *Chin. Phys.* **14** 2061

[13] Hu L Q, Wei M S, Ling B L and Fang Z S 2000 *Plasma Sci. Technol.* **2** 515

[14] Hu L Q, Wan B N, Shi Y J, Yang Y, Gao X, Li J G, Kuang G L, Zhao Y P, Xie J K, Mao J S and Xu Y 2003 *Plasma Phys. Control Fusion* **45** 349

[15] Ma T P, Ruan H L, Hu L Q, Wan B N, Gao X, Zhen X J, Zhou L W, Sun Y W, Gao W, Chen Z Y, Lin S Y and Kong W 2006 *Chin. Phys.* **15** 593

[16] Chen Z Y, Wan B N, Shi Y J and Hu L Q 2006 *Nucl. Instru. Meth. Phys. Res.* A **560** 558

[17] Sajjad S, Gao X, Ling B L, Ti A and Du Q 2008 *Meas. Sci. Technol.* **19** 075701

[18] Esposito B, Bertalot L and Kaschuck Y A 2002 *Nucl. Instru. Meth.* A **476** 522.

[19] Esposito B, Poli F M, Mier J A, Sanchez R and Panaccione L 2003 *Phys. Plasmas* **10** 2350

[20] Martin-Solis J R, Esposito B, Sanchez R and Granucci G 2004 *Nucl. Fusion* **44** 974

[21] Lu H W, Hu L Q, Chen Z Y, Jang Y, Lin S Y and EAST Team 2008 *J. Plasma Phys.* **74** 446

[22] Gao X, Jie Y X, Han X F, Yang Y, Zhang W Y, Xu Q, Liu H Q and Li J G 2008 *Nucl. Fusion* **48** 035009

[23] Yoshino R and Tokuda S 2000 *Nucl. Fusion* **40** 1293

[24] Jaspers R, Finken K H, Mank G, Hoenen F, Boedo J A, Lopescardozo N J and Schuller F C 1993 *Nucl. Fusion* **33** 1775

[25] Knoepfel H, Spong D A, Knoepfel H and Spong D A 1979 *Nucl. Fusion* **19** 785

[26] Chen Z Y, Wan B N, Lin S Y, Shi Y J and Hu L Q 2006 *Phys. Lett.* A **351** 413

[27] Fisch N J and Karney C F F 1985 *Phys. Rev. Lett.* **54** 897

[28] Chen Z Y, Wan B N, Lin S Y, Shi Y J, Hu L Q, Gong X Z, Shan J F, Ding B J, Gao X and HT-7 Team 2006 *Plasma Phys. Control Fusion* **48** 1489

[29] Wan B N, Luo J R, Li J G, Zhao Y P, Shan J F, Bai H Y, Ding B J, Ding Y H, Chen J L, Chen Z Y, Fu P and HT-7 Team 2005 *Nucl. Fusion* **45** S132